

Article

# Tunable Topological Beam Splitter in Superconducting Circuit Lattice

Lu Qi <sup>1</sup>, Yan Xing <sup>1</sup>, Xue-Dong Zhao <sup>1</sup>, Shutian Liu <sup>1,\*</sup>, Xue Han <sup>2</sup>, Wen-Xue Cui <sup>2</sup> and Shou Zhang <sup>2,\*</sup> and Hong-Fu Wang <sup>2,\*</sup>

<sup>1</sup> School of Physics, Harbin Institute of Technology, Harbin 150001, China; qilu\_work@163.com (L.Q.); yanhsing@163.com (Y.X.); 18B911016@hit.edu.cn (X.-D.Z.)

<sup>2</sup> Department of Physics, College of Science, Yanbian University, Yanji 133002, China; xuehan@ybu.edu.cn (X.H.); cuiwenxue@ybu.edu.cn (W.-X.C.)

\* Correspondence: stliu@hit.edu.cn (S.L.); szhang@ybu.edu.cn (S.Z.); hfwang@ybu.edu.cn (H.-F.W.)

**Abstract:** In the usual Su–Schrieffer–Heeger (SSH) model with an even number of lattice sites, the topological pumping between left and right edge states cannot be easily realized since the edge states occupy two-end sites simultaneously. Here we propose a scheme to investigate the topological edge pumping in an even-sized periodically modulated SSH model mapped by a one dimensional superconducting transmission line resonators array. We find that the photon initially prepared in the first resonator can be finally observed at the two-end resonators with a certain proportion. The final photon splitting at the two-end resonators indicates that the present superconducting circuit is expected to realize the topological beam splitter. Further, we demonstrate that the splitting proportion between the two-end resonators can be arbitrarily tuned from 1 to 0, implying the potential feasibility of implementing the tunable topological beam splitter. Meanwhile, we also show that the tunable topological beam splitter is immune to the mild disorder added into the system due to the topology protection of the zero energy modes, and find that the tunable topological beam splitter is much more robust to the global on-site disorder compared with the nearest neighbor disorder. Our work greatly extends the practical application of topological matter in quantum information processing and opens up a new way towards the engineering of topological quantum optical device.

**Keywords:** topological beam splitter; Su–Schrieffer–Heeger model; superconducting circuit lattice



**Citation:** Qi, L.; Xing, Y.; Zhao, X.-D.; Liu, S.-T.; Han, X.; Cui, W.-X.; Zhang, S.; Wang, H.-F. Tunable Topological Beam Splitter in Superconducting Circuit Lattice. *Quantum Rep.* **2021**, *3*, 1–12. <https://dx.doi.org/10.3390/quantum3010001>

Received: 30 November 2020

Accepted: 22 December 2020

Published: 25 December 2020

**Publisher’s Note:** MDPI stays neutral with regard to jurisdictional claims in published maps and institutional affiliations.



**Copyright:** © 2020 by the authors. Licensee MDPI, Basel, Switzerland. This article is an open access article distributed under the terms and conditions of the Creative Commons Attribution (CC BY) license (<https://creativecommons.org/licenses/by/4.0/>).

## 0. Introduction

Topological insulator [1–4] opens up a new way of material classification in condensed matter physics due to the distinct topological construction in geometric space. The inequivalent topological construction leads the topological insulator to support the insulating bulk states and conducting boundary states simultaneously [5–8]. These conducting boundary states are naturally immune to the disorder and perturbation owing to the topological protection caused by energy gap [1–4,9–12]. The special robustness of the boundary states leads them to have various potential applications in quantum optics and quantum information processing [13–16]. For example, based on the topological boundary state, the topological interface state laser can be constructed [17–23], in which the topological laser is protected by the gap and hence immune to the lattice defect. Similarly, the topologically protected boundary states also provide the topological channel to implement the topological state transfer [24–29], which ensures the topological quantum transmission between separated nodes. In addition to the topological boundary states, the topological superconductor usually exhibits the non-localized topological excitation [30–35]. The global fault-tolerant topological quantum computation [36–39] can be naturally constructed if we encode information via these non-localized topological quasi-particles.

Recently, the topological Su–Schrieffer–Heeger (SSH) model [40–43], which can be easily constructed by arranging the dimerized sublattice in one dimensional (1D) space,

has attracted increasing attention due to the structural simplicity and the existence of zero energy topological boundary states. Under the open boundary condition, the translation symmetry of the sublattice is broken, leading to the existence of the boundary states at the two-end sites [42–48]. For example, corresponding to an SSH model with an odd number of lattice sites, the system has a zero energy mode being localized at the leftmost site when the intra-cell coupling is weaker than the inter-cell coupling or being localized at the rightmost site when the intra-cell coupling is larger than the inter-cell coupling. In this way, if we modulate the intra-cell and inter-cell couplings periodically, the zero energy mode in the odd-sized SSH model naturally provides the topological channel to realize the topological edge pumping between topological left and right boundary states [25,49]. However, for the SSH model with the even number of lattice sites, the different open boundary conditions make the SSH model have two boundary states being localized at the both ends of the system simultaneously when the intra-cell coupling is weaker than the inter-cell coupling, resulting in that it seems difficult to realize the topological pumping between the two-end sites because the two-end sites are occupied simultaneously. An effective way to handle the above obstacle is that we introduce the staggered onsite potential, such as the Rice–Mele (RM) pumping [50]. Note that, on the basis of RM pumping, we have realized a topological beam splitter induced by the long-range hopping, in which the initial particle can be finally observed at the first two sites with the approximately equal proportions [51]. The question is that, when the staggered onsite potential and long-range hopping are vanishing, can the similar topological beam splitter still be implemented?

To further explore the confusion mentioned above, in this paper, we propose a scheme to investigate the topological edge state pumping in an SSH chain with the even number of lattice sites, which is mapped by a 1D superconducting transmission line resonators array. We demonstrate that the 1D superconducting transmission line resonators array is equivalent to a periodically modulated SSH model via manipulating the external field. We find that, after a certain time evolution, the photon initially prepared in the first resonator appears in the two-end resonators with a certain proportion simultaneously. We reveal that, if treating the first resonator as one input port and treating the two-end resonators as two output ports, the present superconducting circuit can be mapped into a topological beam splitter (TBS), in which the injected photon at the input port can be finally observed at the two output ports with a certain proportion. Further, we demonstrate that the output proportion between the two output ports can be tuned to an arbitrary value, i.e., from 1 to 0. The tunable TBS has great significance in quantum optics and quantum information processing, such as photon trapping, photon storage, and photon distribution. Our scheme provides a promising and excellent platform to investigate topological quantum information processing and topological quantum optical device.

The paper is organized as follows: In Section 1, we demonstrate the 1D superconducting transmission line resonators array can be mapped into a modulated SSH model with an even number of lattice sites. In Sections 2 and 3, we reveal that the superconducting-circuit-based SSH model is equivalent to a tunable TBS in detail. Finally, a conclusion is given in Section 4.

## 1. Model and Hamiltonian

Consider a 1D transmission line resonators array, as depicted in Figure 1. In this array, two adjacent resonators  $a_n$  ( $a_{n+1}$ ) and  $b_n$  are coupled to each other via the auxiliary superconducting qubit  $Q_1$  ( $Q_2$ ) with the coupling strength  $g_1$  ( $g_2$ ). Note that the energy level space  $\omega_1$  ( $\omega_2$ ) of the superconducting qubit  $Q_1$  ( $Q_2$ ) can be modulated via the magnetic flux provided by a flux-bias line (FBL) [52–54]. Then, the system can be described by the Hamiltonian  $H = H_0 + H_{hop}$  ( $\hbar = 1$ ), with

$$\begin{aligned} H_0 &= \sum_n \left[ \omega_a a_n^\dagger a_n + \omega_b b_n^\dagger b_n + \frac{\omega_1}{2} \sigma_{1,n}^z + \frac{\omega_2}{2} \sigma_{2,n}^z \right], \\ H_{hop} &= \sum_n \left[ g_1 \sigma_{1,n}^+ (a_n + b_n) + g_2 \sigma_{2,n}^+ (a_{n+1} + b_n) + \text{H.c.} \right]. \end{aligned} \quad (1)$$

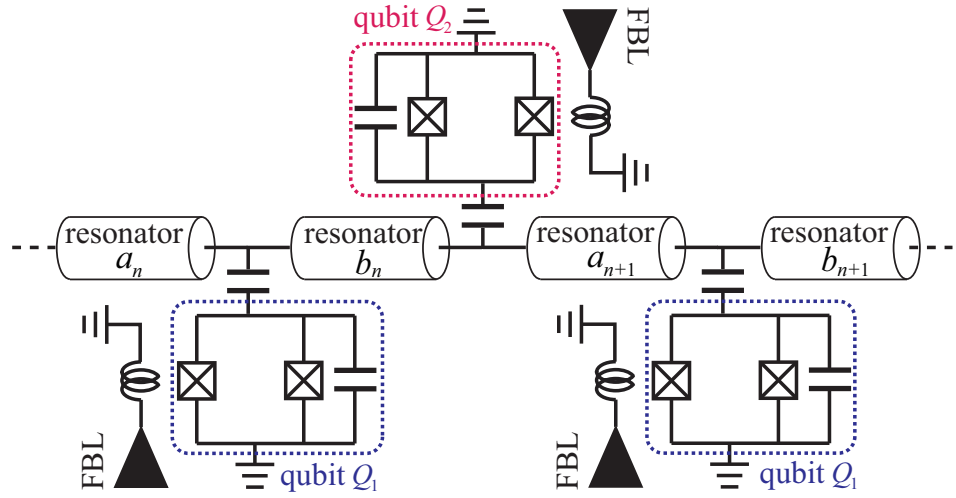


**Figure 1.** The diagrammatic sketch of the 1D transmission line resonators array. The resonators array is composed by  $N$  unit cells (resonators  $a_n$  and  $b_n$  are set as one unit cell), in which the two resonators in a unit cell are coupled to each other via a mediated superconducting qubit  $Q_1$  while the two resonators belonging to two adjacent unit cells are coupled to each other via another mediated superconducting qubit  $Q_2$ . The energy level space of each superconducting qubit can be tuned via magnetic flux provided by a flux-bias line (FBL). The size of the resonators array is  $2N$ .

Here  $H_0$  is the free energy of resonators and qubits with resonator frequency  $\omega_a$  ( $\omega_b$ ) and Pauli  $z$  operator  $\sigma_{1,n}^z = |e\rangle_{1,n}\langle e| - |g\rangle_{1,n}\langle g|$  ( $\sigma_{2,n}^z = |e\rangle_{2,n}\langle e| - |g\rangle_{2,n}\langle g|$ ).  $H_{hop}$  denotes the coupling between two adjacent resonators via qubit  $Q_1$  ( $Q_2$ ), in which  $\sigma_{1,n}^+ = |e\rangle_{1,n}\langle g|$  ( $\sigma_{2,n}^+ = |e\rangle_{2,n}\langle g|$ ) is the excitation of the superconducting qubit  $Q_1$  ( $Q_2$ ), with  $|g\rangle$  and  $|e\rangle$  being the ground and excited states.

In the rotating frame with respect to the external driving frequency  $\omega_d$  and the free energy of qubits, the Hamiltonian in the dispersive regime can be written as  $H' = H'_0 + H'_{hop}$ , with

$$\begin{aligned}
 H'_0 &= \sum_n \Delta_a a_n^\dagger a_n + \Delta_b b_n^\dagger b_n, \\
 H'_{hop} &= \sum_n \frac{g_1^2}{\Delta_1} \left[ (|e\rangle_{1,n}\langle e| a_n a_n^\dagger - |g\rangle_{1,n}\langle g| a_n^\dagger a_n) + (|e\rangle_{1,n}\langle e| b_n b_n^\dagger - |g\rangle_{1,n}\langle g| b_n^\dagger b_n) \right] \\
 &+ \frac{g_2^2}{\Delta_2} \left[ (|e\rangle_{2,n}\langle e| a_n a_n^\dagger - |g\rangle_{2,n}\langle g| a_n^\dagger a_n) + (|e\rangle_{2,n}\langle e| b_n b_n^\dagger - |g\rangle_{2,n}\langle g| b_n^\dagger b_n) \right] \\
 &+ \left[ \frac{g_1^2}{\Delta_1} (|e\rangle_{1,n}\langle e| b_n a_n^\dagger - |g\rangle_{1,n}\langle g| a_n^\dagger b_n) + \frac{g_2^2}{\Delta_2} (|e\rangle_{2,n}\langle e| b_n a_{n+1}^\dagger - |g\rangle_{2,n}\langle g| a_{n+1}^\dagger b_n) + \text{H.c.} \right], \quad (2)
 \end{aligned}$$

where  $\Delta_{i=a,b,1,2} = \omega_i - \omega_d$  is the detuning of the resonators and qubits. Conveniently, the couplings between resonators and qubits can be removed by preparing all the qubits  $Q_{1,n}$  ( $Q_{2,n}$ ) in their ground states, leading to that the total effective Hamiltonian of the system can be expressed as

$$\begin{aligned}
 H_{eff} &= \sum_n \left( \Delta_a - \frac{g_1^2}{\Delta_1} - \frac{g_2^2}{\Delta_2} \right) a_n^\dagger a_n + \left( \Delta_b - \frac{g_1^2}{\Delta_1} - \frac{g_2^2}{\Delta_2} \right) b_n^\dagger b_n \\
 &- \frac{g_1^2}{\Delta_1} (a_n^\dagger b_n + b_n^\dagger a_n) - \frac{g_2^2}{\Delta_2} (a_{n+1}^\dagger b_n + b_n^\dagger a_{n+1}). \quad (3)
 \end{aligned}$$

The first two terms of the above effective Hamiltonian denote the on-site energy assisted by superconducting qubits and the last two terms represent the coupling between two adjacent resonators assisted by qubits. Obviously, the above effective Hamiltonian only

possessing the on-site energy and the nearest neighbor (NN) hopping terms is equivalent to the tight-binding Hamiltonian in form, which provides the basis of the photonic mapping of the topological insulator, such as the photonic SSH model.

As revealed in Figure 1, the energy level space of the superconducting qubits can be tuned via the magnetic flux provided by an external FBL. Thus, the qubits detuning originating from the energy level space of qubits can also be modulated by the external field, such as  $\frac{1}{\Delta_1} = 1 - \cos \theta$  and  $\frac{1}{\Delta_2} = 1 + \cos \theta$ , with  $\theta$  being the modulated parameter in range of  $\theta \in [0, 2\pi]$ . Note that, for simplicity, we set the resonator-qubit coupling  $-g_1^2 = -g_2^2 = 1$  as the energy unit. In this way, after neglecting some constant terms and resetting the energy zero point about the resonator detuning, the final effective Hamiltonian can be written as

$$H_{eff} = \sum_n t_1 a_n^\dagger b_n + t_2 a_{n+1}^\dagger b_n + \text{H.c.}, \quad (4)$$

where the parameters  $t_1 = 1 - \cos \theta$  and  $t_2 = 1 + \cos \theta$  represent the modulated NN hopping strengths, showing that the present 1D transmission line resonators array can be mapped into a modulated photonic SSH model.

For the modulated SSH model with an odd number of lattice sites, there is a zero energy gap state locating in the whole gap, in which the gap state is mainly occupied at the leftmost site when  $t_1 < t_2$  ( $\theta \in [0, 0.5\pi] \cup [1.5\pi, 2\pi]$ ) while it is mainly occupied at the rightmost site when  $t_1 > t_2$  ( $\theta \in [0.5\pi, 1.5\pi]$ ) [25,55]. However, the modulated SSH model with an even number of lattice sites owns two topologically different phases, i.e., the topologically nontrivial phase within  $\theta \in [0, 0.5\pi] \cup [1.5\pi, 2\pi]$  and the topologically trivial phase within  $\theta \in [0.5\pi, 1.5\pi]$ , and has two degenerate zero energy modes in the nontrivial region, as shown in Figure 2a. The distribution of one selected zero energy mode is depicted in Figure 2b–d. The numerical results reveal that the zero energy mode is simultaneously localized at both the ends of the resonators array with the same half of distributions in the most range of  $\theta$  with  $\theta \in [0.1\pi, 0.5\pi] \cup [1.5\pi, 1.9\pi]$ , as shown in Figure 2b. However, the zero energy mode exhibits a completely different distribution pattern at the two-end resonators when  $\theta \sim 0$  ( $\theta \sim 2\pi$ ) with  $\theta \in [0, 0.1\pi]$  ( $\theta \in [1.9\pi, 2\pi]$ ), in which the zero energy mode is simultaneously localized at the two both ends with different distribution proportions, as shown in Figures 2c,d (The different distribution proportions of the zero energy mode at two-end resonators can be seen from the different color patterns in Figure 2c,d).

In the previous investigations about the topological edge pumping in the SSH model [25,49], the topological transfer between the left and right edge states is mainly based on the topological zero energy channel in the SSH model with only the odd number of lattice sites due to the fact that the zero energy mode of the odd-sized SSH model does not occupy the two-end sites simultaneously [49]. Therefore, a question arises: can the topological edge pumping still be realized via the topological zero energy mode in an even-sized SSH chain? This is a natural problem because the distributions of zero energy modes at both ends in the even-sized SSH chain seem to destroy the state transfer channel between the left and right edge states. Especially, the effects of the special state distributions for zero energy modes in  $\theta \in [0, 0.1\pi]$  and  $\theta \in [1.9, 2\pi]$  on the topological edge pumping in the even-sized SSH chain are not yet clearly revealed.

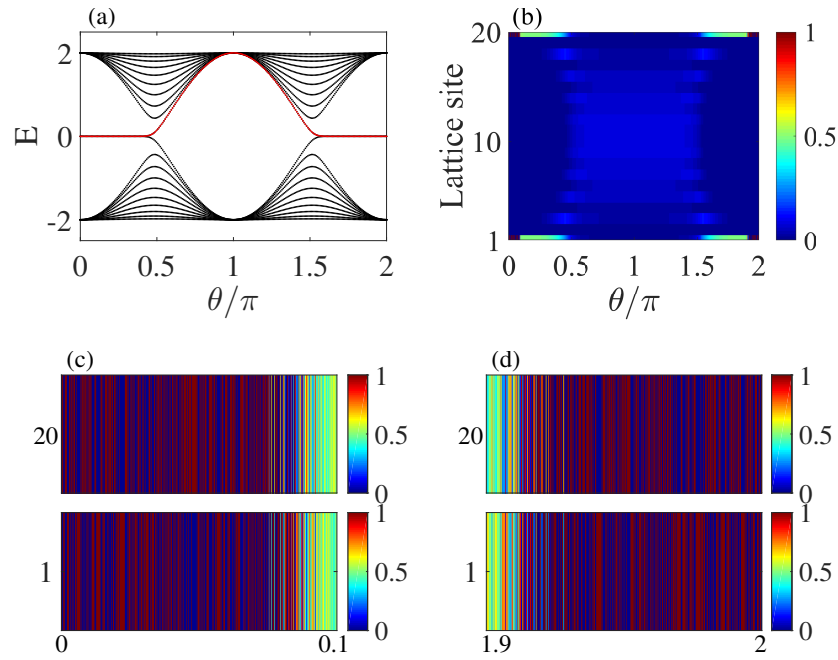


**Figure 2.** The energy spectrum and the distribution of the zero energy mode. (a) The energy spectrum of the even-sized Su–Schrieffer–Heeger (SSH) model. The red line represents the  $(N + 1)$ th eigenvalue versus the periodic parameter  $\theta$ . (b) The eigenstate of the selected zero energy mode (red line in (a)) versus  $\theta$  and lattice site. The detailed distributions of the selected zero energy mode at the two-end resonators are shown in (c) with  $\theta \in [0, 0.1\pi]$  and in (d) with  $\theta \in [1.9\pi, 2\pi]$ . The size of the lattice is  $2N$  with  $N = 10$ . In the unit of  $-g_1^2 = -g_2^2 = 1$ .

## 2. Tunable Topological Beam Splitter

Here, to clarify the above confusion clearly, we rewrite the periodic parameter  $\theta$  as a time-dependent version with  $\theta = \Omega t$ , in which  $\Omega$  represents the varying rate and  $t$  is the time. After that, the Hamiltonian becomes  $H(\theta_t) = \sum_n [1 - \cos(\Omega t)] a_n^\dagger b_n + [1 + \cos(\Omega t)] a_{n+1}^\dagger b_n + \text{H.c.}$ . In order to further explore the feasibility of the topological state transfer in the even-sized SSH array, initially, we prepare the photon in the first resonator and use the time-dependent Hamiltonian  $H(\theta_t)$  to evolve it with  $i \frac{d}{dt} |\Psi\rangle_{\text{initial}} = H(\theta_t) |\Psi\rangle_{\text{initial}}$  [25,49]. The final photon distributions at the two-end resonators versus the varying rate  $\Omega$  are shown in Figure 3a. The detailed patterns of the photon distribution corresponding to different ranges of  $\Omega$  are plotted in Figure 3b–d. The numerical results show that, when  $\Omega$  is quite small, the distributions of photon at two-end resonators exhibit a relatively irregular pattern, as shown in Figure 3b. With  $\Omega$  further increasing, the distributions of photon at the two-end resonator exhibit a regularly periodic pattern, as shown in Figure 3c. Especially, we find that, corresponding to a certain range of  $\Omega$  with the appropriate value, the distribution of the photon in the first resonator  $a_1$  can change from 1 to 0 while the distribution of the photon in the last resonator  $b_N$  changes from 0 to 1 simultaneously. However, when  $\Omega$  is large enough, the maximal distribution of the photon in the first resonator  $a_1$  cannot reach 1, as shown in Figure 3d. These results indicate that, if we choose the varying rate  $\Omega$  appropriately, such as  $\Omega \in [4.530 \times 10^{-3}, 4.554 \times 10^{-3}]$ , the initial photon will appear in the first resonator with the distribution from 1 to 0 accompanied with the distribution in the last resonator from 0 to 1.

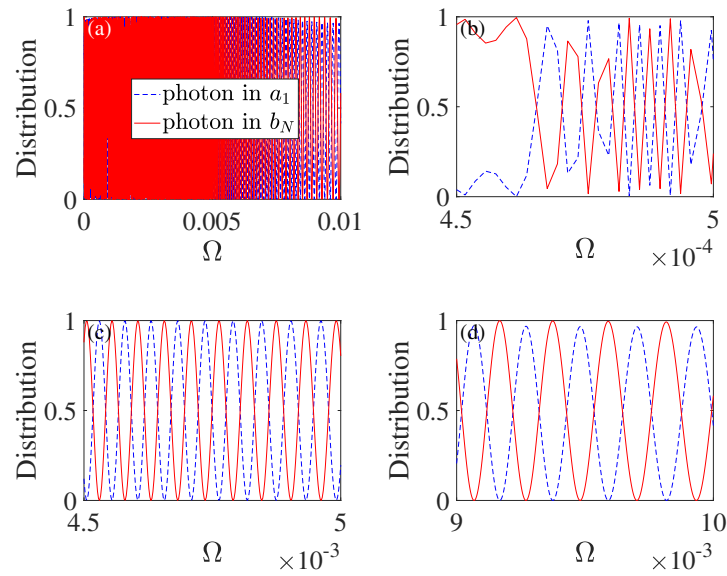


**Figure 3.** (a) The distributions of photons at the two-end resonators for the evolved final state versus the varying rate  $\Omega$ . (b–d) The detailed pattern of the photon distributions at the two-end resonators. The evolution time is  $2\pi/\Omega$ . Other parameter takes  $N = 10$ . In the unit of  $-g_1^2 = -g_2^2 = 1$ .

The above phenomenon illuminates us that, if we treat the first resonator  $a_1$  as one input port and treat the resonators  $a_1$  and  $b_N$  as two output ports, then the photon initially injected into the input port will appear at the two output ports with the certain proportion. We stress that it is feasible and reasonable to treat the resonators as input and output ports since the input and output of each resonator can be individually controlled via the coupled capacitances [52]. The relevant diagrammatic sketch is depicted in Figure 4. Obviously, from the perspectives of photon split-flow device, the present topological SSH-type resonators array can be naturally equivalent to a beam splitter [56–58]. Different from the usual beam splitter, our proposed beam splitter device has two dominant advantages. One is that the present topological SSH-type beam splitter is protected by the topology due to the existence of the zero energy modes, implying that the present beam splitter is a TBS. Thus, the present TBS is naturally immune to the disorder and perturbation added into the system, which has great significance for the realization in experiment. Another advantage is that the splitting proportion between the two output ports can be arbitrarily tuned from 1 to 0, which is different from the usual beam splitter with fixed splitting proportion.

To further verify the feasibility of the TBS, we first prepare the photon at the input port (resonator  $a_1$ ) and numerically simulate the final distributions of photon at the two output ports (resonators  $a_1$  and  $b_N$ ) after a certain time evolution, as shown in Figure 5. The numerical results reveal that the TBS with different splitting proportion can indeed be achieved via choosing different  $\Omega$  appropriately. For example, when  $\Omega = 0.004530$ , we find that the photon initially injected into the input port can be completely exported from the output port 1 after a certain time evolution, as shown in Figure 5a. However, when  $\Omega = 0.004538$  and after a certain time evolution, we find that the photon initially injected into the input port finally appears at the two output ports, as shown in Figure 5b. Especially, the splitting proportion between the output port 1 and output port 2 is 75%:25%, which is totally different from the case in Figure 5a. Similarly, we can also design the TBS with the splitting proportions 50%:50% (Figure 5c), 40%:60% (Figure 5d), 20%:80% (Figure 5e), and even 0%:100% (Figure 5f), via choosing the varying rate  $\Omega$  appropriately. These results indicate that the present SSH-type resonators array can be mapped into a TBS with tunable splitting proportion via modulating the varying rate  $\Omega$ .

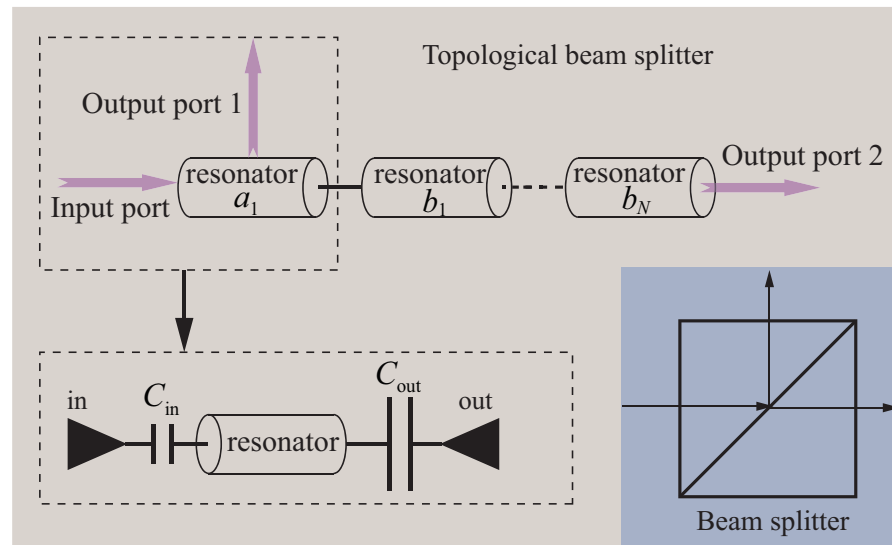


**Figure 4.** The sketch of the topological beam splitter. According to the property that the input and output processes of each resonator can be individually manipulated, the resonators  $a_1$  and  $b_N$  can be regarded as one input port and two output ports. The topological beam splitter has three ports, in which the photons coming from the port 1 and finally appear at port 2 and port 3 with a certain proportion. From this perspective, the present system is equivalent to a beam splitter.

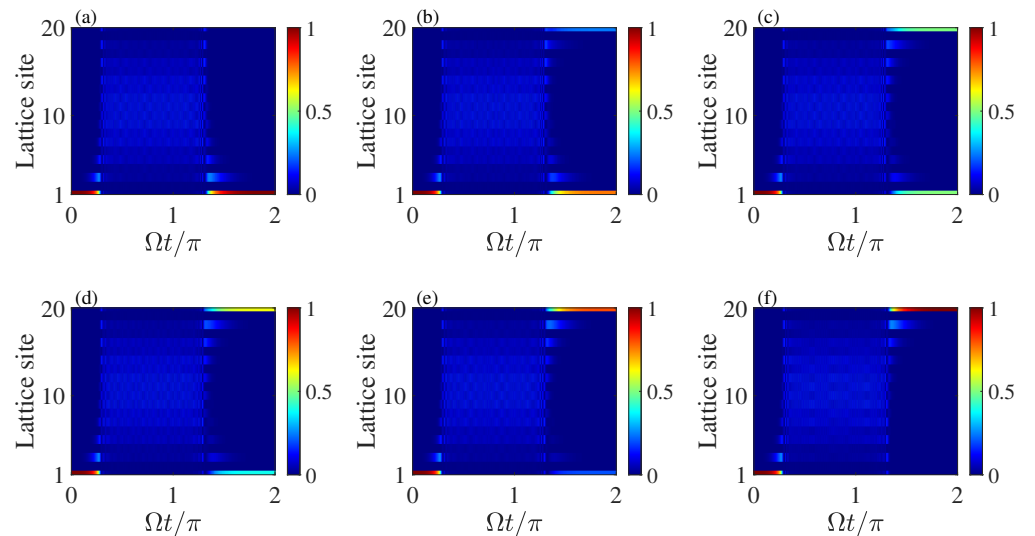


**Figure 5.** The topological beam splitter (TBS) with different splitting proportions when  $\Omega$  takes different values. (a) 100%:0% TBS with  $\Omega = 0.004530$ . (b) 75%:25% TBS with  $\Omega = 0.004538$ . (c) 50%:50% TBS with  $\Omega = 0.0045422$ . (d) 40%:60% TBS with  $\Omega = 0.004544$ . (e) 20%:80% TBS with  $\Omega = 0.0045473$ . (f) 0%:100% TBS with  $\Omega = 0.004554$ . Other parameter takes  $N = 10$ .

We have demonstrated that the tunable TBS can be realized via choosing the appropriate  $\Omega$ , such as the 100%:0% TBS with  $\Omega = 0.004530$  and the 75%:25% TBS with  $\Omega = 0.004538$ . Then a question arises naturally: does the 75%:25% TBS originate from the insufficient evolution caused by the larger  $\Omega = 0.004538$  for a given time? To clarify it, we re-simulate the evolution of different TBSs in Figure 5a–d under the long-time evolution condition, as shown in Figure 6a–d. The numerical results exhibit that the TBS with different splitting proportions can still be achieved under the long-time evolution, implying that the tunable TBS is not caused by the insufficient evolution under the same evolution time. Actually, the TBS with different splitting proportions essentially originates from the eigenstates of the zero energy modes. As revealed in Figure 2c,d, when  $\theta \sim 0$  and  $\theta \sim 2\pi$ ,

the distribution of the zero energy mode exhibits abundant pattern, namely, the zero energy mode has various localized eigenstates with different distributions at the two-ends. These abundant edge eigenstates with different distributions at the two-ends essentially lead to the achievement of the tunable TBS due to the evolution of the eigenstates of the zero energy mode (see DISCUSSION for further discussion).

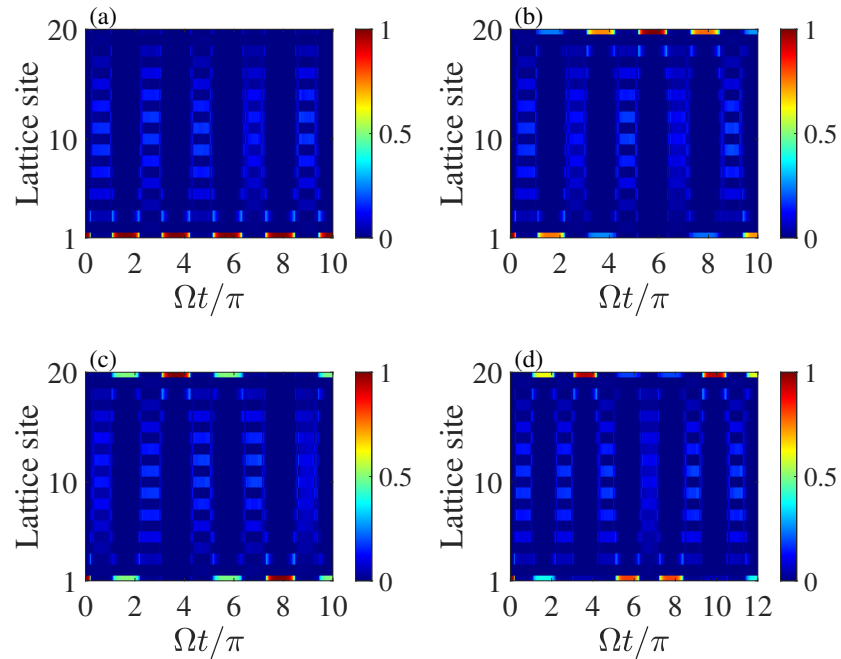


**Figure 6.** The different TBSs in Figure 5a–d under the long time evolution. The TBS can still be achieved under the long time evolution. The parameters are the same as in Figure 5a–d.

The above tunable TBS has numerous potential applications in quantum optics and quantum information processing. For example, the TBS with the splitting proportions 100% : 0% and 0% : 100% can be effectively used to realize the optical trapping or photon storage [59,60], which has great significance in the field of quantum information storage. In addition, the tunable TBS can be readily used to achieve the photon distribution [61,62] with arbitrary proportion for the injected photon source, which is the essential ingredient for entanglement preparation and quantum key distribution in quantum information processing [63,64]. In this way, we can achieve different quantum information processing tasks only based on the tunable TBS device. Note that, depending on the scalability of the transmission line resonators at the single site level, the present tunable TBS can be easily extended to a large scale, which is expected to realize the large scale quantum information processing, such as long-range photon transmission (0%:100% TBS) and photon distributions between two distant nodes (TBS with arbitrary splitting proportion).

As mentioned above, the tunable TBS is assisted by the topological zero energy channel, making that the present tunable TBS is naturally immune to the global disorder  $W\delta$  ( $W$  is the disorder strength and  $\delta$  is the random number in the range of  $[-0.5, 0.5]$ ) added into the system. To further clarify it, under the large enough disorder samples [25], we plot the fidelity of the TBS with different splitting proportions when the disorder is added into the NN hopping and the on-site energy, respectively, as shown in Figure 7. The numerical results reveal that, when the disorder is added into the NN hopping, the fidelity of the TBS exhibits an approximate platform in a certain range of the disorder strength, as shown in Figure 7a. The existence of these platforms indicates that the present TBS is immune to the mild disorder added into the NN hopping. Differently, when the mild disorder is added into the on-site energy, we find that the fidelity almost keeps unchanged with the increasing of the disorder added into the on-site energy, as shown

in Figure 7b. These phenomena imply that the present TBS is much more robust to the on-site disorder compared with the NN disorder since the mild global on-site disorder only makes the energy spectrum move up (down) slightly (cannot change the distributions of the zero energy modes). The topology protection of the tunable TBS greatly facilitates the experimental realization of TBS and provides the possibility for the potential application of topological insulator in quantum optics and quantum information processing.

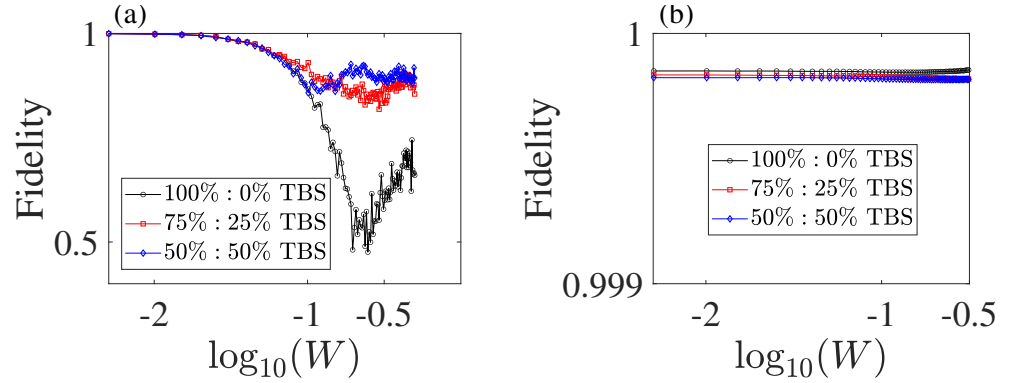


**Figure 7.** The fidelities of different TBSs when the random disorder is added into the system. Note that we neglect the phase information of the evolved final state in the process of calculating the fidelity. (a) The random disorder is added into the nearest neighbor hopping. (b) The random disorder is added into the on-site energy. Other parameter takes  $N = 10$ .

### 3. Discussion

The abundant distribution pattern of the zero energy mode in the region of  $\theta \in [0, 0.1\pi]$  can be interpreted as the following. Note that the matrix of the Hamiltonian for the system under open boundary condition can be expressed as

$$H = \begin{pmatrix} 0 & t_1 & 0 & 0 & \cdots \\ t_1 & 0 & t_2 & 0 & \cdots \\ 0 & t_2 & 0 & t_1 & \cdots \\ 0 & 0 & t_1 & 0 & \cdots \\ \vdots & \vdots & \vdots & \vdots & \ddots \end{pmatrix}. \quad (5)$$

when  $\theta = 0$ , the intra-cell hopping satisfies  $t_1 = 0$ , making the above matrix of Hamiltonian can be easily and analytically solved. Especially, the system has two strict zero energy solutions  $E_{1,2} = 0$  accompanied with two zero energy eigenstates  $|1, 0, 0, \dots, 0, 0\rangle$  and  $|0, 0, 0, \dots, 0, 1\rangle$ , implying the existence of the completely localized left and right edge states. When a finite  $\theta \neq 0$  is added into the system, the intra-cell hopping satisfies  $t_1 \neq 0$ , resulting in the two initial strict zero energy solutions not maintaining the strict zero energy [65]. On the other hand, the two non-strict zero energy solutions weaken the complete localizations of the two edge states. This phenomenon is actually caused by the size effect of the SSH model. More specifically, when  $\theta$  is extremely small, such as  $\theta \in (0, 0.08\pi]$ , the extremely small  $\theta$  corresponds to that  $t_1$  still satisfies  $t_1 \approx 0$ , implying the existence of  $E_{1,2} \approx 0$ , as shown in Figure 8a. The condition of  $E_{1,2} \approx 0$  ensures that the two edge states are still better localized at the two-ends. However, with  $\theta$  continuously increasing, the two initial strict zero energy solutions deviate from the zero energy (see the inset figure of Figure 8a), leading the localizations of the two edge states to be weakened. For example, when  $\theta = 0.089\pi$ , we find that the initial left (right) edge state is mainly localized at the leftmost (rightmost) site accompanied with certain distribution at the rightmost (leftmost) site, implying the destruction of the localization for the left (right) edge state, as shown in Figure 8b. Similarly, with  $\theta$  continuously increasing, the localizations of the two edge states are further weakened and finally reach the same value at the two-end

sites, as shown in Figure 8c,d. The above results reveal that we can always find a finite  $\theta$  in the region of  $[0.08\pi, 0.1\pi]$  to ensure the distributions of the two edge states at the two-ends with the certain proportions. These states with different distribution proportions at the two-ends are the basis to realize the tunable TBS.

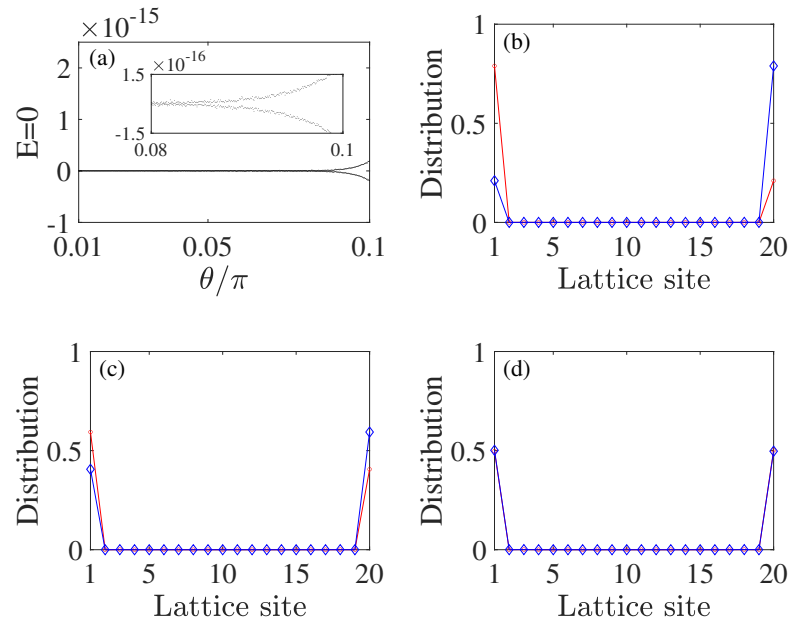


**Figure 8.** The two zero energy eigenvalues and their distributions. (a) The two zero energy eigenvalues versus the parameter  $\theta$ . The inset figure illustrates the detailed pattern for the splitting of the zero energy modes. (b–d) The distributions of two edge states when  $\theta = 0.089\pi$  in (b),  $\theta = 0.095\pi$  in (c), and  $\theta = 0.12\pi$  in (d). The red circle line represents the left edge state and the blue diamond line represents the right edge state. Other parameter takes  $N = 10$ .

#### 4. Conclusions

In conclusion, we have proposed a scheme to investigate the topological edge pumping of the even-sized SSH model based on a 1D superconducting transmission line resonators array. We reveal that the resonators array can be mapped into a topological tight-binding SSH model, in which the NN hopping can be periodically modulated via the external field. We find that, after a certain time evolution in the system, the photon initially prepared in the first resonator appears in the two-end resonators with a certain proportion. We demonstrate that the splitting proportion between the two-end resonators can be tuned to any value from 1 to 0. Depending on the performance that the input and output of the superconducting resonator can be individually manipulated, the present superconducting resonators array is naturally equivalent to a tunable TBS when we regard the first and the two-end resonators as input port and output ports respectively. We further demonstrate that the tunable TBS is immune to the mild disorder added into the system due to the topology protection, which greatly reduces the difficulty of experimental realization. The tunable TBS has various potential applications in quantum optics and quantum information processing. Our scheme provides a new perspective for topological quantum information processing and opens up a new path towards the engineering of topological quantum optical device.

**Author Contributions:** Writing—original draft preparation, L.Q.; software, Y.X. and X.-D.Z.; formal analysis, X.H.; data curation, S.L. and W.-X.C.; investigation, S.Z.; writing—review and editing, H.-F.W. All authors have read and agreed to the published version of the manuscript.

**Funding:** This work was supported by the National Natural Science Foundation of China under Grant Nos. 61822114, 11874132, 61575055, 12074330, and 62071412.

**Conflicts of Interest:** The authors declare no conflict of interest.

## References

1. Hasan, M.Z.; Kane, C.L. Colloquium: Topological insulators. *Rev. Mod. Phys.* **2010**, *82*, 3045. [[CrossRef](#)]
2. Qi, X.L.; Zhang, S.C. Topological insulators and superconductors. *Rev. Mod. Phys.* **2011**, *83*, 1057. [[CrossRef](#)]
3. Chiu, C.K.; Teo, J.C.; Schnyder, A.P.; Ryu, S. Classification of topological quantum matter with symmetries. *Rev. Mod. Phys.* **2016**, *88*, 035005. [[CrossRef](#)]
4. Bansil, A.; Lin, H.; Das, T. Colloquium: Topological band theory. *Rev. Mod. Phys.* **2016**, *88*, 021004. [[CrossRef](#)]
5. Matsuura, S.; Ryu, S. Momentum space metric, nonlocal operator, and topological insulators. *Phys. Rev. B* **2010**, *82*, 245113. [[CrossRef](#)]
6. Wray, L.A.; Xu, S.Y.; Xia, Y.; Hsieh, D.; Fedorov, A.V.; SanHor, Y.; Cava, R.J.; Bansil, A.; Lin, H.; Hasan, M.Z. A topological insulator surface under strong coulomb, magnetic and disorder perturbations. *Nat. Phys.* **2011**, *7*, 32. [[CrossRef](#)]
7. Malki, M.; Uhrig, G. Tunable edge states and their robustness towards disorder. *Phys. Rev. B* **2017**, *95*, 235118. [[CrossRef](#)]
8. Xiao, L.; Zhan, X.; Bian, Z.; Wang, K.; Zhang, X.; Wang, X.; Li, J.; Mochizuki, K.; Kim, D.; Kawakami, N.; et al. Observation of topological edge states in parity–time–symmetric quantum walks. *Nat. Phys.* **2017**, *13*, 1117–1123. [[CrossRef](#)]
9. Bonderson, P.; Nayak, C. Quasi-topological phases of matter and topological protection. *Phys. Rev. B* **2013**, *87*, 195451. [[CrossRef](#)]
10. Paananen, T.; Dahm, T. Magnetically robust topological edge states and flat bands. *Phys. Rev. B* **2013**, *87*, 195447. [[CrossRef](#)]
11. Yong, J.; Jiang, Y.; Usanmaz, D.; Curtarolo, S.; Zhang, X.; Li, L.; Pan, X.; Shin, J.; Takeuchi, I.; Greene, R.L. Robust topological surface state in kondo insulator  $\text{Sb}_2\text{Te}_3$  thin films. *Appl. Phys. Lett.* **2014**, *105*, 222403. [[CrossRef](#)]
12. Takagaki, Y.; Giussani, A.; Perumal, K.; Calarco, R.; Friedland, K.J. Robust topological surface states in  $\text{Sb}_2\text{Te}_3$  layers as seen from the weak antilocalization effect. *Phys. Rev. B* **2012**, *86*, 125137. [[CrossRef](#)]
13. Alicea, J.; Oreg, Y.; Refael, G.; VonOppen, F.; Fisher, M.P. Non-abelian statistics and topological quantum information processing in 1D wire networks. *Nat. Phys.* **2011**, *7*, 412. [[CrossRef](#)]
14. Duclos-Cianci, G.; Poulin, D. Fast decoders for topological quantum codes. *Phys. Rev. Lett.* **2010**, *104*, 050504. [[CrossRef](#)]
15. Bonderson, P.; Lutchyn, R.M. Topological quantum buses: Coherent quantum information transfer between topological and conventional qubits. *Phys. Rev. Lett.* **2011**, *106*, 130505. [[CrossRef](#)]
16. Kim, I.H. Long-range entanglement is necessary for a topological storage of quantum information. *Phys. Rev. Lett.* **2013**, *111*, 080503. [[CrossRef](#)]
17. Parto, M.; Wittek, S.; Hodaei, H.; Harari, G.; Bandres, M.A.; Ren, J.; Rechtsman, M.C.; Segev, M.; Christodoulides, D.N.; Khajavikhan, M. Edge-mode lasing in 1D topological active arrays. *Phys. Rev. Lett.* **2018**, *120*, 113901. [[CrossRef](#)]
18. Qiao, J.; Zhao, S.; Yang, K.; Song, W.H.; Qiao, W.; Wu, C.L.; Zhao, J.; Li, G.; Li, D.; Li, T.; et al. High-quality 2- $\mu\text{m}$  Q-switched pulsed solid-state lasers using spin-coating-coreduction approach synthesized  $\text{Bi}_2\text{Te}_3$  topological insulators. *Photon. Res.* **2018**, *6*, 314–320. [[CrossRef](#)]
19. Pilozzi, L.; Conti, C. Topological lasing in resonant photonic structures. *Phys. Rev. B* **2016**, *93*, 195317. [[CrossRef](#)]
20. Bandres, M.A.; Wittek, S.; Harari, G.; Parto, M.; Ren, J.; Segev, M.; Christodoulides, D.N.; Khajavikhan, M. Topological insulator laser: Experiments. *Science* **2018**, *359*, eaar4005. [[CrossRef](#)]
21. Harari, G.; Bandres, M.A.; Lumer, Y.; Rechtsman, M.C.; Chong, Y.D.; Khajavikhan, M.; Christodoulides, D.N.; Segev, M. Topological insulator laser: Theory. *Science* **2018**, *359*, eaar4003. [[CrossRef](#)] [[PubMed](#)]
22. Knitter, S.; Liew, S.F.; Xiong, W.; Guy, M.I.; Solomon, G.S.; Cao, H. Topological defect lasers. *J. Opt.* **2015**, *18*, 014005. [[CrossRef](#)]
23. Sobon, G. Mode-locking of fiber lasers using novel two-dimensional nanomaterials: Graphene and topological insulators [invited]. *Photon. Res.* **2015**, *3*, A56–A63. [[CrossRef](#)]
24. Dłaska, C.; Vermersch, B.; Zoller, P. Robust quantum state transfer via topologically protected edge channels in dipolar arrays. *Quantum Sci. Technol.* **2017**, *2*, 015001. [[CrossRef](#)]
25. Mei, F.; Chen, G.; Tian, L.; Zhu, S.L.; Jia, S. Robust quantum state transfer via topological edge states in superconducting qubit chains. *Phys. Rev. A* **2018**, *98*, 012331. [[CrossRef](#)]
26. Leijnse, M.; Flensberg, K. Quantum information transfer between topological and spin qubit systems. *Phys. Rev. Lett.* **2011**, *107*, 210502. [[CrossRef](#)]
27. Ni, R.; Niu, Y.; Du, L.; Hu, X.; Zhang, Y.; Zhu, S. Topological charge transfer in frequency doubling of fractional orbital angular momentum state. *Appl. Phys. Lett.* **2016**, *109*, 151103. [[CrossRef](#)]
28. Kraus, Y.E.; Lahini, Y.; Ringel, Z.; Verbin, M.; Zilberberg, O. Topological states and adiabatic pumping in quasicrystals. *Phys. Rev. Lett.* **2012**, *109*, 106402. [[CrossRef](#)]
29. Tangpanitanon, J.; Bastidas, V.M.; Al-Assam, S.; Roushan, P.; Jaksch, D.; Angelakis, D.G. Topological pumping of photons in nonlinear resonator arrays. *Phys. Rev. Lett.* **2016**, *117*, 213603. [[CrossRef](#)]
30. Linder, J.; Tanaka, Y.; Yokoyama, T.; Sudbø, A.; Nagaosa, N. Unconventional superconductivity on a topological insulator. *Phys. Rev. Lett.* **2010**, *104*, 067001. [[CrossRef](#)]
31. Papić, Z.; Bernevig, B.A.; Regnault, N. Topological entanglement in abelian and non-abelian excitation eigenstates. *Phys. Rev. Lett.* **2011**, *106*, 056801. [[CrossRef](#)] [[PubMed](#)]
32. Pal, P.B. Dirac, majorana, and weyl fermions. *Am. J. Phys.* **2011**, *79*, 485–498. [[CrossRef](#)]
33. Beenakker, C. Search for majorana fermions in superconductors. *Annu. Rev. Condens. Matter Phys.* **2013**, *4*, 113–136. [[CrossRef](#)]
34. Lutchyn, R.M.; Sau, J.D.; Sarma, S.D. Majorana fermions and a topological phase transition in semiconductor-superconductor heterostructures. *Phys. Rev. Lett.* **2010**, *105*, 077001. [[CrossRef](#)] [[PubMed](#)]

35. Sato, M.; Fujimoto, S. Topological phases of noncentrosymmetric superconductors: Edge states, majorana fermions, and non-abelian statistics. *Phys. Rev. B* **2009**, *79*, 094504. [[CrossRef](#)]
36. Sarma, S.D.; Freedman, M.; Nayak, C. Majorana zero modes and topological quantum computation. *NPJ Quantum Inf.* **2015**, *1*, 15001. [[CrossRef](#)]
37. Stern, A.; Lindner, N.H. Topological quantum computation from basic concepts to first experiments. *Science* **2013**, *339*, 1179–1184. [[CrossRef](#)]
38. Aasen, D.; Hell, M.; Mishmash, R.V.; Higginbotham, A.; Danon, J.; Leijnse, M.; Jespersen, T.S.; Folk, J.A.; Marcus, C.M.; Flensberg, K.; et al. Milestones toward majorana-based quantum computing. *Phys. Rev. X* **2016**, *6*, 031016. [[CrossRef](#)]
39. Tewari, S.; Sarma, S.D.; Nayak, C.; Zhang, C.; Zoller, P. Quantum computation using vortices and majorana zero modes of a  $p_x + ip_y$  superfluid of fermionic cold atoms. *Phys. Rev. Lett.* **2007**, *98*, 010506. [[CrossRef](#)]
40. Kivelson, S.; Heim, D. Hubbard versus peierls and the Su-Schrieffer-Heeger model of polyacetylene. *Phys. Rev. B* **1982**, *26*, 4278. [[CrossRef](#)]
41. Fradkin, E.; Hirsch, J.E. Phase diagram of one-dimensional electron-phonon systems. i. the Su-Schrieffer-Heeger model. *Phys. Rev. B* **1983**, *27*, 1680. [[CrossRef](#)]
42. Meier, E.J.; An, F.A.; Gadway, B. Observation of the topological soliton state in the Su-Schrieffer-Heeger model. *Nat. Commun.* **2016**, *7*, 13986. [[CrossRef](#)] [[PubMed](#)]
43. Li, L.; Xu, Z.; Chen, S. Topological phases of generalized Su-Schrieffer-Heeger models. *Phys. Rev. B* **2014**, *89*, 085111. [[CrossRef](#)]
44. DiLiberto, M.; Recati, A.; Carusotto, I.; Menotti, C. Two-body physics in the Su-Schrieffer-Heeger model. *Phys. Rev. A* **2016**, *94*, 062704. [[CrossRef](#)]
45. Lieu, S. Topological phases in the non-hermitian Su-Schrieffer-Heeger model. *Phys. Rev. B* **2018**, *97*, 045106. [[CrossRef](#)]
46. Capone, M.; Stephan, W.; Grilli, M. Small-polaron formation and optical absorption in Su-Schrieffer-Heeger and holstein models. *Phys. Rev. B* **1997**, *56*, 4484. [[CrossRef](#)]
47. Asbóth, J.K.; Oroszlány, L.; Pályi, A. The su-schrieffer-heeger (SSH) model. In *A Short Course on Topological Insulators*; Springer: Berlin/Heidelberg, Germany, 2016; pp. 1–22.
48. Grusdt, F.; Höning, M.; Fleischhauer, M. Topological edge states in the one-dimensional superlattice Bose-Hubbard model. *Phys. Rev. Lett.* **2013**, *110*, 260405. [[CrossRef](#)] [[PubMed](#)]
49. Qi, L.; Wang, G.L.; Liu, S.; Zhang, S.; Wang, H.F. Controllable photonic and phononic topological state transfers in a small optomechanical lattice. *Opt. Lett.* **2020**, *45*, 2018–2021. [[CrossRef](#)]
50. Rice, M.J.; Mele, E.J. Elementary excitations of a linearly conjugated diatomic polymer. *Phys. Rev. Lett.* **1982**, *49*, 1455–1459. [[CrossRef](#)]
51. Qi, L.; Wang, G.L.; Liu, S.; Zhang, S.; Wang, H.F. Engineering the topological state transfer and topological beam splitter in an even-sized Su-Schrieffer-Heeger chain. *Phys. Rev. A* **2020**, *102*, 022404. [[CrossRef](#)]
52. Schmidt, S.; Koch, J. Circuit QED lattices: Towards quantum simulation with superconducting circuits. *Ann. Phys.* **2013**, *525*, 395–412. [[CrossRef](#)]
53. Manucharyan, V.E.; Koch, J.; Glazman, L.I.; Devoret, M.H. Fluxonium: Single cooper-pair circuit free of charge offsets. *Science* **2009**, *326*, 113–116. [[CrossRef](#)] [[PubMed](#)]
54. Manucharyan, V.E.; Masluk, N.A.; Kamal, A.; Koch, J.; Glazman, L.I.; Devoret, M.H. Evidence for coherent quantum phase slips across a josephson junction array. *Phys. Rev. B* **2012**, *85*, 024521. [[CrossRef](#)]
55. Begum, S.; Fleurov, V.; Kagalovsky, V.; Yurkevich, I.V. Sliding Luttinger liquid with alternating interwire couplings. *J. Phys. Condens. Matter* **2019**, *31*, 425601. [[CrossRef](#)] [[PubMed](#)]
56. Jonckheere, T.; Rech, J.; Zazunov, A.; Egger, R.; Martin, T. Hanbury brown and twiss noise correlations in a topological superconductor beam splitter. *Phys. Rev. B* **2017**, *95*, 054514. [[CrossRef](#)]
57. Wang, X.S.; Su, Y.; Wang, X.R. Topologically protected unidirectional edge spin waves and beam splitter. *Phys. Rev. B* **2017**, *95*, 014435. [[CrossRef](#)]
58. Schonbrun, E.; Wu, Q.; Park, W.; Yamashita, T.; Summers, C.J. Polarization beam splitter based on a photonic crystal heterostructure. *Opt. Lett.* **2006**, *31*, 3104–3106. [[CrossRef](#)]
59. Maxwell, D.; Szwed, D.J.; Paredes-Barato, D.; Busche, H.; Pritchard, J.D.; Gauguier, A.; Weatherill, K.J.; Jones, M.P.A.; Adams, C.S. Storage and control of optical photons using rydberg polaritons. *Phys. Rev. Lett.* **2013**, *110*, 103001. [[CrossRef](#)]
60. Yanik, M.F.; Fan, S. Dynamic photon storage. *Nat. Phys.* **2007**, *3*, 372–374. [[CrossRef](#)]
61. Takesue, H.; Nam, S.W.; Zhang, Q.; Hadfield, R.H.; Honjo, T.; Tamaki, K.; Yamamoto, Y. Quantum key distribution over a 40-db channel loss using superconducting single-photon detectors. *Nat. Photonics* **2007**, *1*, 343–348. [[CrossRef](#)]
62. Ball, P.; Braun, V.; Kivel, N. Photon distribution amplitudes in QCD. *Nucl. Phys. B* **2003**, *649*, 263–296. [[CrossRef](#)]
63. Rosenfeld, W.; Berner, S.; Volz, J.; Weber, M.; Weinfurter, H. Remote preparation of an atomic quantum memory. *Phys. Rev. Lett.* **2007**, *98*, 050504. [[CrossRef](#)] [[PubMed](#)]
64. Torres, J.P.; Deyanova, Y.; Torner, L.; Molina-Terriza, G. Preparation of engineered two-photon entangled states for multidimensional quantum information. *Phys. Rev. A* **2003**, *67*, 052313. [[CrossRef](#)]
65. Yuce, C. Robust bulk states. *Phys. Lett. A* **2019**, *383*, 1791–1794. [[CrossRef](#)]